High Energy Physics and Nuclear Physics

Volume 21, Number 2

Static Theory for Nuclear Multifragmentation I. Phase Transition and Multifragmentation

Zhang Fengshou and Ge Lingxiao

(Institute of Modern Physics, The Chinese Academy of Sciences, Lanzhou, China)

With a density-, temperature-, and momentum-dependent mean field, five different phases of nuclear equation of states (gas, liquid, super-heated liquid, super-cooled gas, and mechanical instability of the spinodal phase) for ^{197}Au are described. After performing a simulation in coordinate space and in momentum space for these different phases at finite temperature $T = 6$ MeV, all kinds of nuclear clusters are sorted by using the coalescence model. The correlation analysis of the nuclear clusters demonstrates that the multifragmentation pattern only comes from the mechanical instability of the spinodal phase.

Key words: equation of state, mechanical instability of spinodal phase, multifragmentation.

Received March 12, 1996.

1. INTRODUCTION

The process that the highly excited nuclei formed in intermediate heavy ion collisions decay into many intermediate mass fragments (IMFs) with charge $Z \geq 3$ and light particles is referred to as the multifragmentation. Extensive studies have been carried out throughout the world to provide a better understanding of this process [1-10]. Its underlying properties are, however, not yet clear. One may believe that the multifragmentation is related to some general features in nature such as scaling properties.

Theoretical investigations have been developed along two different lines: the microscopic dynamic approaches [7-10] and the phenomenological static models [4-6]. The dynamic approaches are able to describe an entire process from the initial stage to the multifragmentation; the molecular dynamics model [7] and nuclear transport theory [8] cannot, however, really describe the multifragmentation because of the problems in the model or the problems of the numerical methods used. The recently developed stochastic nuclear transport theory which incorporates dynamic fluctuations is considered as a promising dynamic model for the nuclear multifragmentation [9-10], but progress is slow because of its great numerical demands. In contrast, because of the complexity in the final stage of collisions, the phenomenological static models such as the statistic model, are quite successful in describing certain aspects of the multifragmentation [4-6].

In this paper, a static nuclear multifragmentation model is developed. The properties of hot nuclei formed in intermediate energy heavy ion collisions and the possible phase transition, multifragmentations, the critical behavior, and intermittency are studied based on this model.

2. THEORETICAL MODEL

2.1. Equation of states and phase transitions of finite nucleus ^{197}Au

We start with the extended Skyrme force [11], which is a density and momentum dependent effective interaction. In nuclear matter, the single particle wave function is given by a plane wave. The single particle distribution function at temperature T in the phase space is given by the Fermi-Dirac distribution:

$$f_{\pm}(r, p) = \frac{1}{1+e^{\frac{\frac{p^2}{2m_{\pm}} - \mu_{\pm}}{T}}} , \tag{1}$$

The index $\pm$ of the quantities denotes the neutron and proton parts, respectively. The chemical potentials $\mu_{\pm}$ for neutrons and protons are given by:

$$\rho_{\pm} = \frac{g}{(2\pi\hbar)^3} \int_0^{\infty} d^3p \, \frac{1}{1+e^{\frac{\frac{p^2}{2m_{\pm}} - \mu_{\pm}}{T}}} , \tag{2}$$

here g is a degeneracy factor. In the Hartree-Fock approximation [12], one obtains the density, temperature, and momentum dependent mean field as follows [13]:

$$U_{\pm} = a_{\pm}^{(1)}\rho + a_{\pm}^{(2)}\rho^{\gamma+1} + a_{\pm}^{(3)}\rho^{\frac{5}{3}} + a_{\pm}^{(4)}\rho^{\gamma+\frac{5}{3}} , \tag{3}$$

where,

$$
\begin{cases}
a_{\pm}^{(1)} = \dfrac{1}{4}\, t_0[3 \mp (2x_0+1)\alpha] \,, \\
a_{\pm}^{(2)} = \dfrac{1}{24}\, t_3[3 \mp (2x_3+1)\alpha] \,, \\
a_{\pm}^{(3)} = \dfrac{1}{16\pi^2}\,[t_1(1-x_1)+3t_2(1+x_2)](1\pm\alpha)^{\frac{5}{3}}\left(\dfrac{2\sqrt{\pi}}{\lambda}\right)^5 C_{\frac{3}{2}}(\mu_{\pm}) \\
\quad + \dfrac{1}{8\pi^2}\left[t_1\left(1+\dfrac{x_1}{2}\right)+t_2\left(1+\dfrac{x_2}{2}\right)\right](1\mp\alpha)^{\frac{5}{3}}\left(\dfrac{2\sqrt{\pi}}{\lambda}\right)^5 C_{\frac{3}{2}}(\mu_{\mp}) \,, \\
a_{\pm}^{(4)} = \dfrac{1}{16\pi^2}\,[t_4(1-x_4)+3t_5(1+x_5)](1\pm\alpha)^{\frac{5}{3}}\left(\dfrac{2\sqrt{\pi}}{\lambda}\right)^5 C_{\frac{3}{2}}(\mu_{\pm}) \\
\quad + \dfrac{1}{8\pi^2}\left[t_4\left(1+\dfrac{x_4}{2}\right)+t_2\left(1+\dfrac{x_5}{2}\right)\right](1\mp a)^{\frac{5}{3}}\left(\dfrac{2\sqrt{\pi}}{\lambda}\right)^5 C_{\frac{3}{2}}(\mu_{\mp}) \,.
\end{cases}
\tag{4}
$$

where $\gamma = 1/6$, $t_0 = -2635$ MeVfm^3, $t_1 = 385$ MeVfm^5, $t_2 = -120$ MeVfm^5, $t_3 = 15595$ MeVfm$^{3+3\gamma}$, $t_4 = 0$ MeVfm^8, $t_5 = 0$ MeVfm^8, and $x_0 = 0.09$, $x_1 = 0$, $x_2 = 0$, $x_3 = 0$, $x_4 = 0$, and $x_5 = 0$ are the SKM parameters of the Skyrme force, α, λ, and $C_v(\mu_{\pm})$ represent the asymmetry parameter, the thermal wavelength, and the Fermi-Dirac integral, respectively,

$$\alpha = \frac{\rho_+ - \rho_-}{\rho} \,, \tag{5}$$

$$\lambda = \hbar^2\sqrt{\frac{2\pi}{mT}} \,, \tag{6}$$

$$C_v(\mu_{\pm}) = \int_0^{\infty} dx \frac{x^v}{1+e^{x-\frac{\mu_{\pm}}{T}}} \,. \tag{7}$$

For finite nuclei, by considering the Coulomb and surface effects one obtains the following single nucleon energy,

$$
\begin{aligned}
\varepsilon(\rho,\, T) = {} & a_s^0\left(1+\frac{3}{2}\,\frac{T}{T_c}\right)\left(1-\frac{T}{T_c}\right)^{\frac{2}{3}} \rho_0^{\frac{3}{2}} A^{-\frac{1}{3}} \rho^{\frac{1}{3}} + 0.348(1-\alpha)^2 A^{\frac{2}{3}} \rho^{\frac{1}{3}} \\
& + \frac{1}{2}\, T\left[\frac{C_{\frac{3}{2}}(\mu_+)}{C_{\frac{1}{2}}(\mu_+)}\,(1+\alpha)^{\frac{5}{2}} + \frac{C_{\frac{3}{2}}(\mu_-)}{C_{\frac{1}{2}}(\mu_-)}\,(1-\alpha)^{\frac{5}{2}}\right] \\
& + \frac{1}{4}\,[a_+^{(1)}(1+\alpha)+a_-^{(1)}(1-\alpha)]\rho \\
& + \frac{1}{4}\,[a_+^{(2)}(1+\alpha)+a_-^{(2)}(1-\alpha)]\rho \\
& + \frac{1}{4}\,[a_+^{(3)}(1+\alpha)+a_-^{(3)}(1-\alpha)]\rho \\
& + \frac{1}{4}\,[a_+^{(4)}(1+\alpha)+a_-^{(4)}(1-\alpha)]\rho \,,
\end{aligned}
\tag{8}
$$

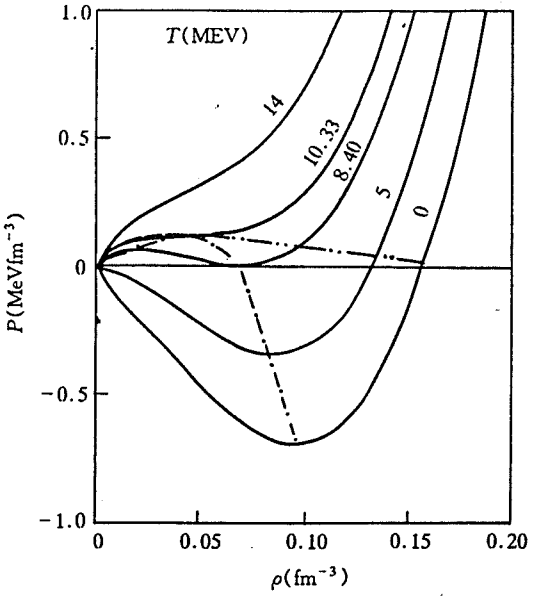

Fig. 1

Pressure-density isotherms for the finite nucleus ^{197}Au.
—··— is for the liquid-gas coexistence line; —·— is for the mechanical instability line.

where a_s^0 is the parameter of the surface energy term in the liquid drop model [14], T_c is the critical temperature for the liquid-gas phase transition, and ρ_0 is the density of the ground state. From Eq. (8) one can generate the ground state properties of infinite nuclear mater for different sets of the Skyrme force [13]. The parameters of the SKM force will be used in this paper to give the ground state effective mass $\frac{m^*}{m} = 0.79$ and the ground state compression coefficient $K = 215.5$ MeV. The pressure-density isotherms for ^{197}Au are shown in Fig. 1. The critical point is defined as that in thermodynamics. The limiting point is defined as the highest value of temperature at which the pressure becomes negative. This is the maximum temperature of the finite nucleus. For ^{197}Au, the critical point is at $T_c = 10.33$ MeV and $\rho_c = 0.045$ fm^{-3}, while the limiting point is at $T_l = 8.40$ MeV and $\rho_l = 0.070$ fm^{-3}. Similar works can be found in Refs. [15-20].

2.2. Numerical simulations

The isotherms in the $P-\rho$ phase diagram in Fig. 1 allow one to identify five regions: the gas phase, the liquid phase, the super-heated liquid phase, the super-cooled gas phase region, and the mechanically unstable spinodal phase. For very energetic collisions, the pressure remains positive for all densities. Therefore, one can describe the process as an instantaneous vaporization, with a relatively small fraction of composite particles in the final state. This is shown in the high temperature part of Fig. 1. In the lower temperature region of the isotherm the pressure is negative. As the expansion slows down in this region all will come to halt when all the collective kinetic energy converts into the internal energy. Thus the system will oscillate back and forth along the isotherms. In these two cases, there are no phase transitions. If there is a separation between a condensed phase and a vapor phase, the thermodynamics becomes more complicated. The usual liquid-gas phase transition is a first-order

transition that applies to processes occurring slowly enough for an equilibrium to be established across the phase boundary in the system. The phase transition time scale is of the order of the evaporation time, but the dynamic expansion is much faster. One may, however, consider a second possibility for the breakup of the expanding system, the expansion is so rapid that the two phase equilibrium cannot be established. Then the expansion proceeds along the curves of constant temperature into the domain of metastable super-heated states as shown in Fig. 1. This transient regime is special also because it exhibits negative pressure. For a thermodynamically stable state it has the largest entropy and lowest free energy. The mechanically unstable system will expand until it reaches the minimum in $P(\rho, T)$, and multifragments will be formed by the many-body effects and then bounded by the mean field.

At the last stage of the real heavy ion collisions it may enter different regions of the P-ρ phase diagram. The problem now is how to make realistic simulations of these states. We map the entire P-ρ phase space for different density ρ and temperature T, and then simulate each point (ρ, T) in a realistic way. One can select a point (ρ, T) in each region and sample it as follows.

(1) At temperature $T = 0$ MeV, we sample for proton and neutron, respectively, in coordinate and momentum spaces as follows,

$$\begin{aligned} \rho(r) &= \theta(R-r)\,\rho \ , \\ f(p) &= \theta(P_F-p) \ , \end{aligned} \tag{9}$$

where $R = \sqrt[3]{\frac{3A}{4\pi\rho}}$ is the bulk radius and $P_F = \hbar\sqrt[3]{\frac{3}{2}\pi^2\rho}$ is the Fermi momentum. From Fig. 2, one can see that 100 events can reach a realistic simulation.

(2) In the cases of $T > 0$ MeV, we sample in coordinate and momentum spaces as follows:

$$\begin{aligned} \rho(r) &= \theta\ (R\ (T)-r)\rho \ , \\ f(p) &= \frac{1}{1+e^{\frac{\frac{p^2}{2m}-\mu}{T}}} \ , \end{aligned} \tag{10}$$

where $R(T) = \sqrt[3]{\frac{3A}{4\pi\rho}}\ (1 + 0.0005T^2)$ is adopted from a thermal Hartree-Fock calculation [16] and μ can be obtained from Eq. (2).

Note that here we actually simulate the nucleon distribution in r-space and in p-space in the final stage of the reaction. This is independent of the models. From the distributions described above, we can determine all kinds of fragments in different regions of Fig. 1 by the coalescence model. We use the 6-dimension coalescence model to determine the formation of IMFs as in Ref. [21]. Here we adopt a parameter set of $r_0 = 3.0$ fm and $p_0 = 200$ MeV/c.

3. MULTIFRAGMENTATION ANALYSIS

From the definitions of the thermodynamic equilibrium and the mechanically unstable lines, one can identify that, for ^{197}Au at $T = 6$ MeV, the densities for the mechanically unstable region, the super-heated liquid region, and the hot liquid region are in the range of 0.01—0.07 fm^{-3}, 0.08—0.11 fm^{-3}, and 0.12—0.15 fm^3, respectively. We use $T = 6$ MeV because this line crosses all the regions. The analysis for different temperatures will be addressed in a separate publication.

Measuring the charge multiplicity is a conventional method in the investigation of the nuclear multifragmentation. However, only the correlation measurement can give a real signal of the multifragmentation. In Fig. 4, we show the charge distributions of all fragments (Fig. 4a) and the

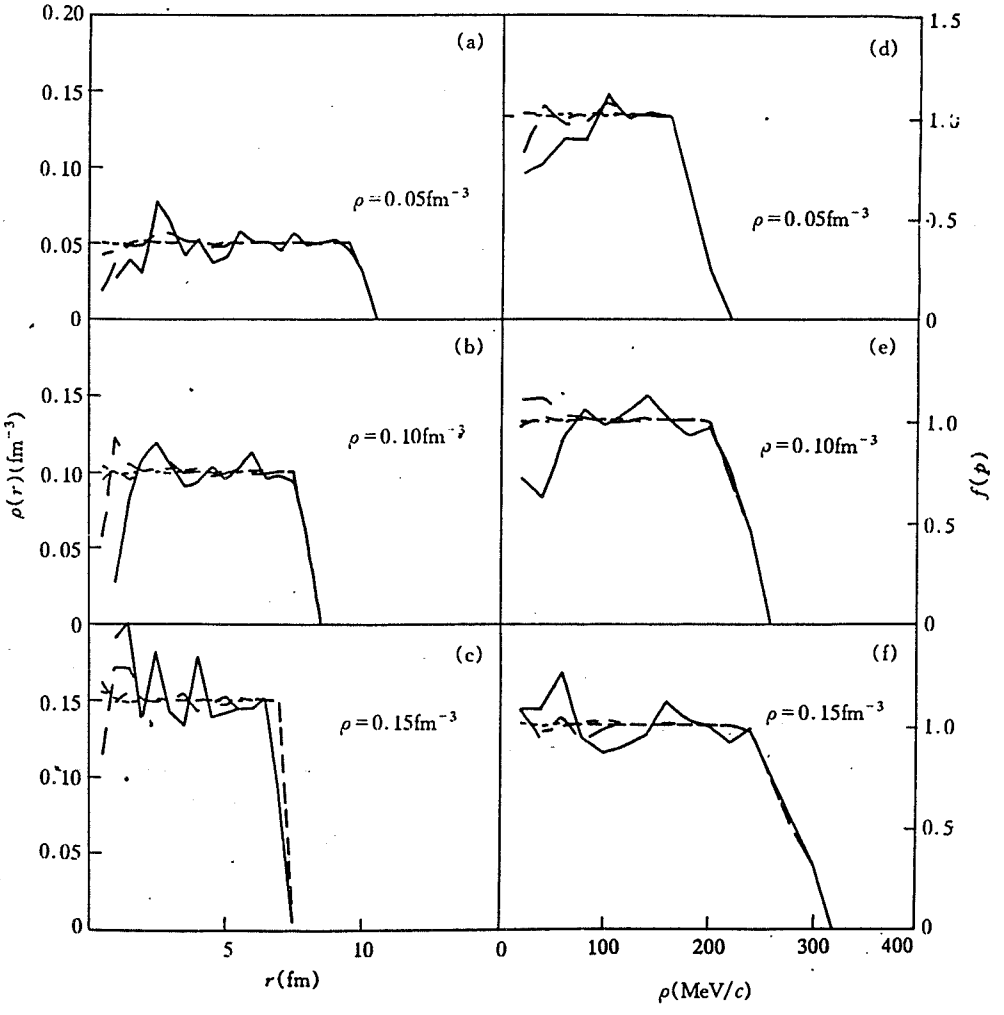

Fig. 2
The mean distributions of ^{197}Au in r-space (a-c) and in p-space (d-f), at $T = 0$.
Numbers of events: ——10; —— 100; ----- 1000; ····· 10000.

correlation between the multiplicity of IMF and Z_{bound} (Fig. 4b), for the mechanically unstable phase, the super-heated liquid, the hot liquid regions, and their mixing for ^{197}Au at $T = 6$ MeV. Z_{bound} is the sum of the charges of all fragments with $Z \geq 2$ and the IMF is defined for fragments with $3 \leq Z \leq 20$ in this study. In the density range 0.01—0.15 fm^{-3}, which is produced in the expansion process of heavy ion collisions, there are two peaks which correspond to large clusters and light-charged particles, respectively. Note that the window of the spinodal phase, namely $\rho = 0.01$—0.07 fm^{-3}, provides most of the produced IMFs. In contrast, the hot liquid region $\rho = 0.12$—0.15 fm^{-3} and the $\rho = 0.08$—0.11 fm^{-3} region provide most of the large clusters. The spectra of the light particles and IMF can be fitted by a power law distribution $M_Z \propto Z^{-\tau}$, with $\tau = 2.53 \pm 0.15$, 2.43 ± 0.16, 1.64 ± 0.13, and 1.91 ± 0.20 for $\rho = 0.01$—0.15, 0.01—0.07, 0.08—0.11 and 0.12—0.15 fm^{-3}, respectively. One can see that $\tau = 2.53 \pm 0.15$ corresponds to the mixed events and $\tau = 2.43 \pm 0.16$ for the spinodel phase are close to the experimental results [2].

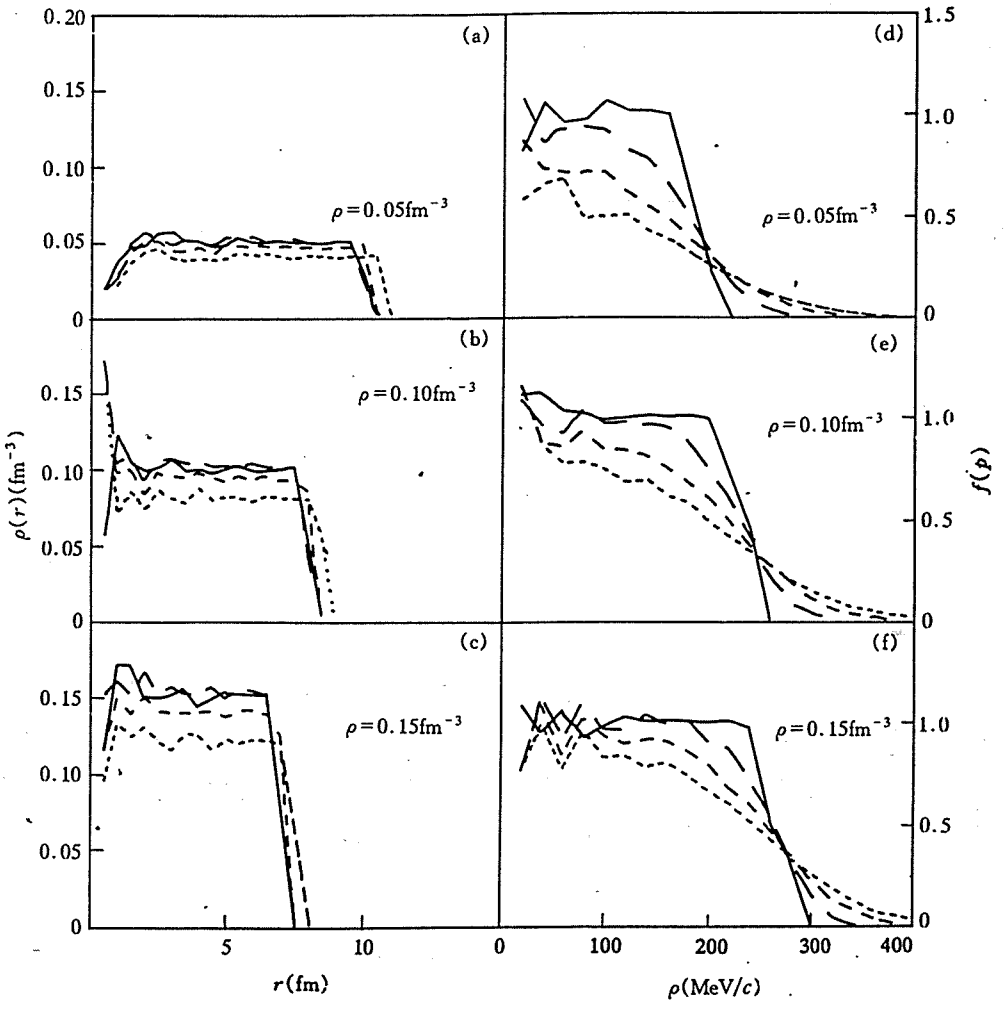

Fig. 3
The mean distributions of ^{197}Au in r-space (a-c) and in p-space (b-d) at different temperatures.
—— $T = 0$ MeV; —— $T = 5$ MeV; ---- $T = 10$ MeV; and ····· $T = 15$ MeV.

As mentioned above, only from the correlation analysis can one get a signal of the multi-fragmentation. The smaller values of Z_{bound} correspond to the events with many light nuclear fragments and the larger values correspond to the events with only one big fragment. Both of them are normal decays. From Fig. 4b, one can see that M_{IMF} is larger than 2 in the region of $Z_{\text{bound}} = 22$—65. The maximum value of the IMF multiplicity can reach 9 at $Z_{\text{bound}} = 40$ and 56 for $\rho = 0.01$—0.15fm^{-3}. By comparing the curves in different regions, one observes that the curve in the spinodal region in the range of $Z_{\text{bound}} = 22$—65 has the same behavior as the M_{IMF} curve. This means that the contributions from the super-heated liquid phase and the hot liquid phase to $M_{\text{IMF}} \geq 2$ are only from the $Z_{\text{bound}} \geq 66$ region. One can conclude that the IMFs come from the spinodal region, i.e., multifragmentation is due to the mechanical instability.

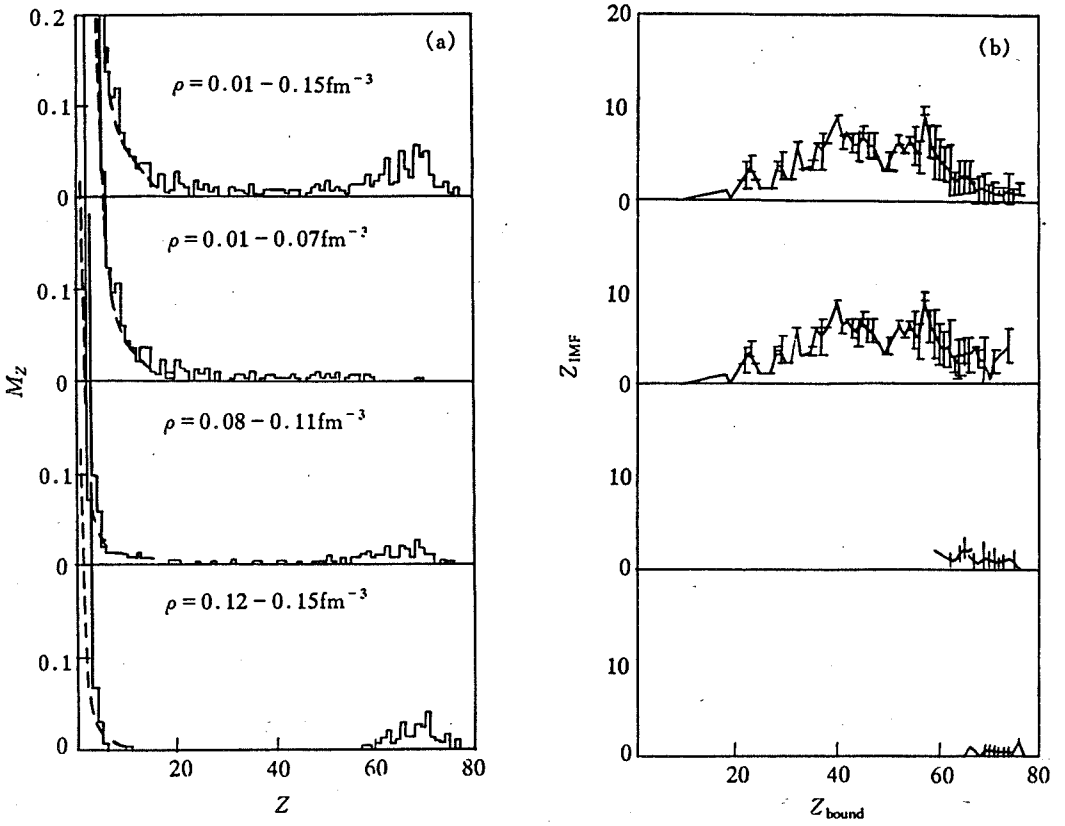

Fig. 4

The charge distributions of all fragments and the power law fit (dashed lines) (a) and the correlation between the multiplicity of IMF and Z_{bound} (b) for the spinodal, the super-heated liquid, the hot liquid phases, and their mixing for ^{197}Au at $T = 6$ MeV.

4. CONCLUSION

A static multifragmentation model is developed in this paper. With a density-, temperature-, and momentum-dependent mean field, we described five different phases of the nuclear equation of states: gas, liquid, super-heated liquid, super-cooled gas, and mechanical instability of spinodal phase at typical temperature $T = 6$ MeV. The isotherm can cross the liquid, super-heated liquid, and mechanical instability of spinodal phases. From realistic simulations in r-space and p-space for these different phase regions for ^{197}Au, we studied all kinds of nuclear clusters by using a coalescence model. From the correlation analyses of these nuclear clusters, we found that the multifragmentation comes from the mechanically unstable spinodal region.

There have been many investigations about the generic features in the multifragmentation. This work suggests that the mechanically unstable spinodal phase of the nuclear equation of states is responsible for the pattern of the multifragmentation in intermediate-energy heavy ion collisions. We will discuss in our future work whether this conclusion provides some hints for basic laws in nature, such as critical behavior and intermittency.

REFERENCES

[1] D.R. Bowman *et al.*, *Phys. Rev. Lett.*, **67**(1991), p. 1527.
[2] C.A. Ogilvie *et al.*, *Phys. Rev. Lett.*, **67**(1991), p. 1214.
[3] G. Bizard *et al.*, *Phys. Lett.*, **B302**(1993), p. 162.
[4] M. Ploszajczak and A. Tucholski, *Phys. Rev. Lett.*, **65**(1990), p. 1539.
[5] X. Campi, *Phys. Lett.*, **B208**(1988), p. 351.
[6] D.H.E. Gross and Sa-Ben Hao, *Nucl. Phys.*, **A437**(1985), p. 643.
[7] J. Aichelin, *Phys. Rep.*, **202**(1991), p. 233.
[8] G.F. Bertsch and S. Das Gupta, *Phys. Rep.*, **160**(1988), p. 189.
[9] F.S. Zhang and E. Suraud, *Phys. Lett.*, **B319**(1993), p. 35.
[10] F.S. Zhang and E. Suraud, *Phys. Rev.*, **C51**(1995), p. 2301.
[11] L.X. Ge, Y.Z. Zhou, and W. Nörenberg, *Nucl. Phys.*, **A459**(1986), p. 77.
[12] P. Ring and P. Schuck, The Nuclear Many-Body Problem, Berlin: Springer-Verlag, 1980.
[13] F.S. Zhang and L.X. Ge, *High Energy Phys. and Nucl. Phys.* (Chinese Edition), **16**(1992), p. 666.
[14] W.D. Myers and W.J. Swiatecki, *Ann. of Phys.*, **55**(1969), p. 355.
[15] G.F. Bertsch and P.J. Siemens, *Phys. Lett.*, **B126**(1983), p. 9.
[16] G. Sauer, H. Chandra and U. Mosel, *Nucl. Phys.*, **A264**(1976), p. 221.
[17] J. Randrup and E.L. Medeiros, *Nucl. Phys.*, **A529**(1991), p. 115.
[18] E. Suraud, *Nucl. Phys.*, **A462**(1987), p. 109.
[19] C. Ngô, H. Ngô, S. Leary *et al.*, *Nucl. Phys.*, **A499**(1989), p. 148.
[20] S. Shlomo and J.B. Natowitz, *Phys. Rev.*, **C44**(1991), p. 2878.
[21] H. Kruse, B. Jacak, J. Molitoris *et al.*, *Phys. Rev.*, **C31**(1985), p. 1770.